6 Acoustic phonons on Y(0001)/W(110)

This chapter presents the laser-induced electron and lattice dynamics on the Y(0001)/W(110) system, investigated with time-resolved linear reflectivity and second-harmonic generation techniques. Of central importance here is the encountered phenomenon of travelling acoustic phonons within the Y(0001) thin film, the so-called *phonon echo*. The chapter is structured as follows. After a brief presentation of the characteristic properties of the investigated system Y(0001)/W(110), the physics of phonon echo and its vast area of applications are introduced. The theoretical model used to describe the phono echo dynamics is detailed in the following section. In the next step we present the measured phonon echo dynamics on the the Y(0001) films and the way is reflected in the transient linear reflectivity. More insight in the physics of the phonon echo is gained by varying the temperature of the system and the laser wavelength. Concluding remarks and an outlook to the future work are closing the chapter.

6.1 Introduction

The motivation that triggers the investigation of the second rare-earth system in this work is to test the accumulated knowledge in the case of gadolinium regarding the excitation of coherent lattice motion and presumably to get more insight into the physics of quasiparticle excitations and interactions. From the previous chapter we have seen that the main ingredients in excitation and detection of coherent lattice vibrations at the surface are: a crystalline structure that can support optical branch phonons, an electronic configuration resembling an exchange-split surface state through which an efficient excitation of the surface lattice motion can be achieved and a surface sensitive tool that can detect these coherent lattice vibrations. In this context yttrium is a good candidate since is a rare-earth metal [18, 19] that crystallizes in a hcp structure with two atoms per unit cell, having the values of the lattice constants close to Gd metal. Thus the first condition is fulfilled, the measured phonon dispersion curves [167] for yttrium showing at Γ point a frequency of 4.6 THz for the longitudinal optical phonons. Similar to gadolinium, yttrium is a trivalent metal $(4d5s)^3$ *i.e.* has the same valence electronic structure and exhibiting a surface state which is now positioned at the E_F (see figure 6.6). Unlike Gd, the surface state is not exchange-split since Y is a paramagnet *i.e.* shows no long-range magnetic ordering. As investigation tools we employ here the time-resolved second-harmonic generation together with linear reflectivity. Hence, we can check wheatear on yttrium one can initiate coherent lattice vibrations in the THz frequency range.

Phonon echo

The concept of phonon echo denotes a propagating acoustic phonon wavepacket through a medium, being reflected at the buried (medium/substrate) interface or at any discontinuity in the material and at the free surface. As it travels, the acoustic pulse modulates locally the optical properties of the system, which can be monitored with *e.g.* time-resolved linear optical techniques as a change in the reflectivity or transmission measured in the transient signal. The back and forth travelling within the sample (see fig. 6.1) of the acoustic pulse is reflected in the transient signal as sharp peaks (see fig. 6.7), which appear at regular time intervals accounting for the propagating time through the sample. Because these peaks represent replica of the initially generated acoustic pulse, this phenomenon is known as *phonon echo* by analogy to the spin-echo process.

The propagating acoustic pulse or sound wave can be excited mechanically by a piezoelectric transducer attached to the investigated specimen or optically by absorption of ultrashort laser pulses that heats up the lattice which expands and thus generating a strain pulse. The latter method allows generation of acoustic pulses in the GHz frequency range whereas with the former one MHz frequencies (the practical limit of driving electronics is below 1 GHz) can be obtained. The technique of the laser-induced propagating acoustic pulses is known as *picosecond ultrasonics* or *laser ultrasonics* [168, 169] due to the ability to generate acoustic pulses with temporal extents in the picosecond time scale.

A schematic picture of the laser-induced strain pulses is presented in the figure 6.1. Initially the pump pulse is absorbed within a distance given by the optical penetration depth. The photoexcited electrons will transfer their energy to the lattice which will be heated up and expand. Thermal expansion of the lattice produces the strain pulse (its shape will be discussed later in this section) that travels through the sample being partially reflected and transmitted at the buried interface and totally reflected with a sign change at the free surface.Its presence is detected by the time-delayed probe pulse as a temporally change (see fig. 6.7) in the relative variations of the measured signal (reflectivity, transmission etc.).

A big advantage of the optically generated acoustic pulses represents the capability of performing *non-contact*, *non-invasive* and *non-destructive* measurements, which with the conventional ultrasonic techniques is impossible. Because of these characteristics the laser ultrasonics is widely use in industry in general [170] and is particularly useful in the semiconductor industry [171] for measurements and quality characterization of multilayered thin films and microstructures. Also this technique can investigate specimens held at elevated temperatures, located in corrosive and hostile environments etc. Moreover, the phonon echo effect exhibits a large variety of applications ranging from medical investigation to determination of thin film thickness and mechanical properties (sound velocity, bulk modulus) [172] and from diagnostics of various materials [173] to imaging nano-objects in embedded structures [174]. These are just a few areas where the laser ultrasonics is applied and the extensive literature covering these fields can not be cited here. The interested reader is referred to the work of Scruby [168] and Gusev [169], that give a wider overview of the research field.

In general, for the generation of the high frequency acoustic pulses metallic films are used due to the relatively short optical penetration depth and the rapid response of the

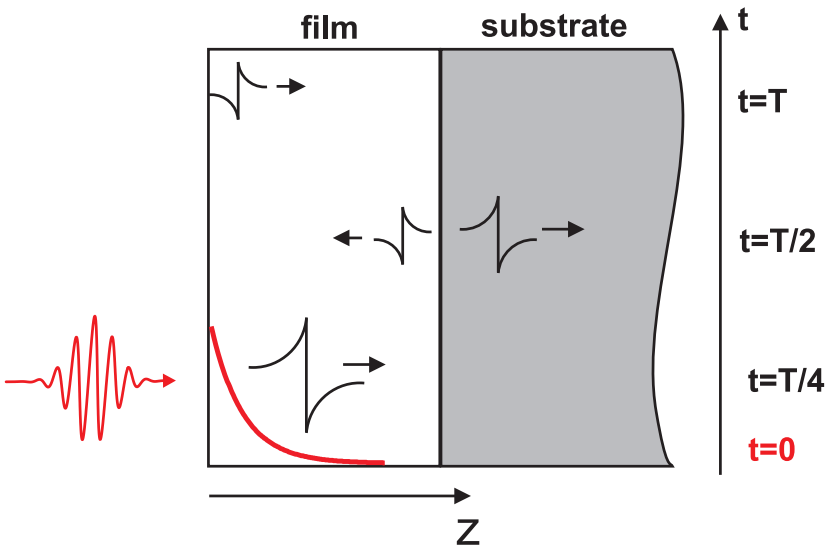

Figure 6.1: Schematic illustration of the laser-induced generation and propagation of the strain pulse within a film/substrate system. At t=0 the laser pulse is absorbed in the limit of the optical penetration depth that produces a temperature increase having the distribution of the absorption profile. At a later time the generated strain pulse travels to the buried interface where is partially reflected and transmitted. Arriving at the free surface the strain pulse is reflected with a sign change. The arrows indicate the propagating direction of the strain pulse.

lattice to the electronic excitation. In a first approximation, the frequency content of the excited acoustic pulse is limited by the spatial extent of the optical penetration depth. However, the initial absorption profile of the laser pulse can be broadened by the ballistic and diffusive electron transport or even by the heat diffusion into the sample. Based on these facts a reverse investigation can be performed namely from the detected phonon echoes the shape of the strain pulse can be inferred and consequently information about the electron dynamics and the magnitude of the electron-phonon coupling can be deduced [175, 176].

The phenomenon of propagating strain pulse should not be mixed with the acoustic shock wave. The latter one is also a travelling strain pulse but with different characteristics namely high amplitude and very short durations. Due to the high amplitudes of the strain the deformation of the lattice is so large that the travelling velocity *i.e.* sound velocity starts to depend on the local pressure within the pulse. As a result we assist at a *self-steepening* of the strain pulse since the sound velocity increases with the increase of the locally applied pressure. Consequently the peak of the strain pulse travels faster and even overtakes the leading trail of the pulse and thus creating a shock wave.

The most use investigation technique for the measurement of the propagating strain pulse is the time-resolved linear reflectivity. Here the changes produced in the optical constants of the material by the strain pulse upon pump pulse absorption are detected in the near-surface region by the time-delayed probe pulse. In the present thesis we employ

this technique for the detection of the phonon echo on Y(0001). Another technique that measures actually the change in the geometry of the surface created by the strain pulse arriving at the surface is the beam deflection technique [44, 177]. With this technique one measures beside the changes in the reflectivity also the deflection of the probe beam produced by the local tilting of the surface plane produced by the strain pulse. A more advanced interferometric technique has been recently introduced [176], that renders simultaneously information about the magnitude and phase of the modulations produced in the linear reflectivity by the propagating acoustic pulse.

6.2 Thermoelastic model

In this section the theoretical model accounting for the optical excitation, propagation and detection of the strain pulse is described. This model has been proposed for the first time by Thomsen *et al.* [178], the description presented here following in some parts the original work of Thomsen. The thermoelastic model is presented in detail here since it provides a thorough understanding of the laser excitation, propagation and detection of the phonon echo process.

6.2.1 Acoustic pulse generation and propagation

In the following the absorption of an ultrafast laser pulse at the surface of a metal film and the subsequent excitation and propagation of the strain pulse is modelled.

The absorption of the laser pulse in the material take place within the optical penetration depth δ defined in eq. 2.3. The variation of the laser intensity along z direction, where z is along the surface normal, has an exponential profile with the characteristic length of the penetration depth (see figure 6.1):

$$I(z) = I_0(1-R)exp\left(-\frac{z}{\delta}\right) \tag{6.1}$$

Here R denotes the reflectivity and I_0 is the incident laser intensity. The absorbed energy from the pump pulse per unit volume at a distance z for an uniformly irradiated area A reads [178]:

$$E(z) = (1-R)\frac{E_p}{A\delta}exp\left(-\frac{z}{\delta}\right) \tag{6.2}$$

with E_p being the energy per laser pulse. Accounting for the expression of the energy per pulse $E_p = I \cdot A \cdot \tau_p$ one can write eq. 6.2 in terms of laser pulse duration τ_p as:

$$E(z) = (1-R)\frac{I_0\tau_p}{\delta}exp\left(-\frac{z}{\delta}\right) \tag{6.3}$$

The absorbed energy produces a temperature increase of the lattice, which resembles the gradient of the absorption profile, and can be written as:

$$\Delta T(z) = \frac{E(z)}{C} = (1-R)\frac{I_0\tau_p}{\delta\rho c}exp\left(-\frac{z}{\delta}\right) \tag{6.4}$$

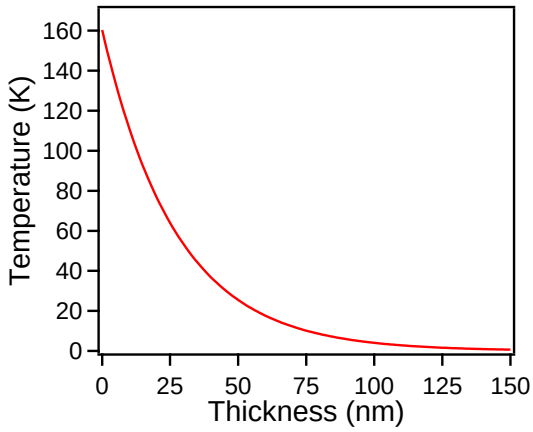

Figure 6.2: Calculated temperature gradient along film thickness upon laser pulse absorption using eq. 6.4 for the case of a yttrium thin film.

Property	Yttrium	Tungsten
density[kg/m^3]	4472	19250
sound velocity[m/s]	3300	5174
reflectivity (775 nm)	0.19	–
penetration depth[nm] (775 nm)	28.7	23
linear expansion coefficient[K^{-1}] (100 K)	13.6e-6	2.6e-6
Poisson ratio	0.24	0.28
bulk modulus[GPa]	41	310
specific heat [J/m^{3}K]	300	–
thermal conductivity [W/mK]	17.2	170

Table 6.1: The physical properties used in the simulation of the propagating strain pulse within the framework of the thermoelastic model.

where $C = \rho \cdot c$ is the specific heat per unit volume determined by the density ρ and the specific heat capacity c of the material.

In the figure 6.2 we show the calculated temperature increase with the expression 6.4 in the case of a yttrium film. We have used a pulse duration τ_p=35 fs and a fluence of $1mJ/cm^2$. The other values of the parameters involved in the calculation are listed in table 6.1. We observe a relatively high temperature increase of 160 K which is mainly determined by the high optical absorption (R=0.19 at 775 nm laser wavelength) of the yttrium film. Also we notice that the temperature gradient is extended on a spatial extent covering approximately three times the penetration depth δ=28.68 nm.

The increased temperature of the material results in a thermal expansion of the lattice and consequently to the appearance of a thermal stress σ_{therm} that will set up a lattice strain η. The relationship between stress and strain is similar to applied force-resulting effect connection since the stress is defined as force per area and the strain is the resulting lattice displacement $\frac{\partial u}{\partial z}$ [135], with u the equilibrium lattice coordinate.

Before we proceed with the description of the thermoelastic model is worthwhile to make some remarks. In metals the penetration depth is in order of 10–30 nm, that is much smaller than the laser spot diameter, usually in the μm range. Thus the lateral extension of the thermoelastic source is much bigger than its spatial extent along z axis. Accounting for the diffusive heat transport out of the irradiated region during the laser pulse duration one obtains a travel distance $l_{diff} = \sqrt{D\tau_p}$ [175], where $D = K/C$ is thermal diffusivity and K is thermal conductivity. For yttrium l_{diff} amounts to ≈0.66 nm which much smaller than skin depth. Also during the laser pulse the produced strain can travel over a distance $l_{ap} = v\tau_p$ (v is the sound velocity), that for yttrium amounts to 0.115 nm again much smaller than δ. Based on these observations we can consider the initial temperature distribution as being homogeneously distributed in the plane of the sample and exponentially decaying along z. Consequently the resulting strain tensor η has only one component that should be considered namely along z direction, η_z, and thus the thermoelastic model has an one-dimensional character. In our further deductions we consider the stress and strain with components just along z direction.

The expression of the induced stress, for an elastically isotropic medium, consists of two components that denote the normal mechanical stress and a component induced by the lattice heating:

$$\sigma_z = \sigma_{mech} + \sigma_{therm} = 3\frac{1-\nu}{1+\nu}B\eta_z - 3B\alpha\Delta T(z) \tag{6.5}$$

with ν, B and α representing the Poisson ratio, bulk modulus and the linear expansion coefficient, respectively.

Solving eq. 6.5 together with the equation of motion along z direction

$$\rho\frac{\partial^2 u_z}{\partial t^2} = \frac{\partial \sigma_z}{\partial z} \tag{6.6}$$

and with the expression of the strain tensor

$$\eta_z = \frac{\partial u_z}{\partial z} \tag{6.7}$$

the spatial and temporal profile of the propagating strain pulse is obtained [178]:

$$\eta_z(z,t) = (1-R)\frac{I_0\tau_p\alpha}{\delta\rho c}\frac{1-\nu}{1+\nu}\left[e^{-\frac{z}{\delta}}\left(1-\frac{1}{2}e^{-\frac{vt}{\delta}}\right) - \frac{1}{2}e^{\frac{-|z-vt|}{\delta}}sgn(z-vt)\right] \tag{6.8}$$

The strain pulse travels with the longitudinal sound velocity v of the material, that is defined as:

$$v = \sqrt{3\frac{1-\nu}{1+\nu}\frac{B}{\rho}} \tag{6.9}$$

The above obtained strain expression is plotted in the figure 6.3 for the yttrium case at different instances in time. We see that the strain contains a time-dependent part denoting the propagating acoustic pulse that is described by the second term in eq. 6.11, and a time-independent component located in the near-surface region caused by the initial laser-induced thermal expansion. The propagating part of the strain pulse consists of two

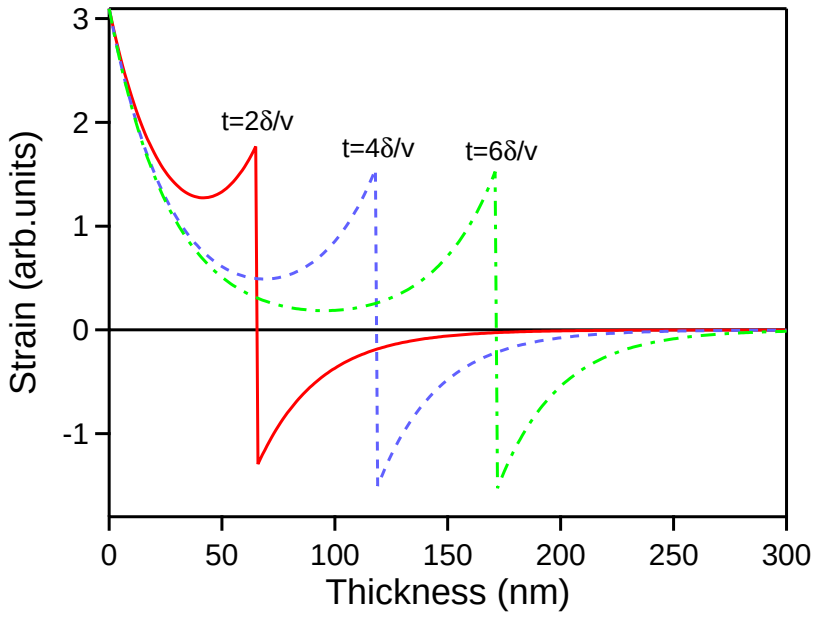

Figure 6.3: Illustration of the resulting strain pulse at different time instances as it travels through the Y(0001) thin film.

components of equal magnitude and opposite sign. During the laser pulse absorption one part is travelling along positive direction of z axis (the component with negative strain) while the other part goes to the negative direction (-z) being instantaneously reflected at the free surface with a sign change.

As it travels through the sample the strain pulse is partially reflected and partially transmitted at the film/substrate interface with a certain factor r_{fs} while at the free surface it will be totally reflected with a change in polarity. The factor r_{fs} denotes the acoustic reflection coefficient that is defined as:

$$r_{fs} = \frac{Z_s - Z_f}{Z_s + Z_f} \tag{6.10}$$

where $Z_i = \rho \cdot v$ represents the acoustic impedance for the film and the underlying substrate. The magnitude of r_{fs} gives how much from the travelling acoustic pulse is reflected at the film-substrate interface and its sign giving the polarity of the strain pulse.

Accounting just for the propagating part of the strain pulse one can write expression 6.11 as:

$$\eta_z(z,t) = (1-R)\frac{I_0\tau_p\alpha}{\delta\rho c}\frac{1-\nu}{1+\nu}r_{fs}\left[\frac{1}{2}e^{\frac{-|z+vt|}{\delta}}sgn(z+vt) + \frac{1}{2}e^{\frac{-|z-vt|}{\delta}}sgn(z-vt)\right] \tag{6.11}$$

with the first term describing the strain component with negative sign and the second term the positive strain component.

6.2.2 Acoustic pulse detection

The laser-induced variations in the linear reflectivity of the system will consist in this case of a temperature (electron and lattice) induced component and changes produced by the travelling strain pulse that modulates locally the optical properties of the system. In the following we focus on the detection of the strain-induced changes in the optical reflectivity. Generally, one can write both effects as giving a change in the linear reflectivity as:

$$\Delta R = \mid r + \Delta r \mid^2 - \mid r \mid^2 \tag{6.12}$$

with r being the reflectivity of the system in equilibrium and Δr the modulation of the LR due to the presence of strain. The dielectric constant is given by $\epsilon = (n + ik)^2$ where n and k represent the real and the imaginary part of the refractive index. The produced changes of the optical constant by the propagating acoustic pulse are given by:

$$\Delta n(z,t) = \frac{\partial n}{\partial \eta_z}\eta_z(z,t) \tag{6.13}$$

$$\Delta k(z,t) = \frac{\partial k}{\partial \eta_z}\eta_z(z,t) \tag{6.14}$$

$$\tag{6.15}$$

where $\frac{\partial n}{\partial \eta_z}$ and $\frac{\partial k}{\partial \eta_z}$ represent the photoelastic constants. These values are very rare in the literature (no reports for yttrium) and are also wavelength dependent [179] and might change the polarity of the phonon echo pulse. Thus we can write the variation of the dielectric constant due to the presence of strain as:

$$\Delta\epsilon(z,t) = 2(n+ik)\left(\frac{\partial n}{\partial \eta_z} + i\frac{\partial k}{\partial \eta_z}\right)\eta_z(z,t) \tag{6.16}$$

The final expression of the strain-induced changes in the linear reflectivity is given by [178]:

$$\Delta R = \int_0^\infty f(z)\eta_z(z,t)dz \tag{6.17}$$

Here $f(z)$ is the so-called sensitivity function that quantifies the contribution of the strain being situated at different depths below the surface to the detected linear reflectivity:

$$f(z) = f_0\left[\frac{\partial n}{\partial \eta_z}sin\left(\frac{4\pi nz}{\lambda} - \phi\right) + \frac{\partial k}{\partial \eta_z}cos\left(\frac{4\pi nz}{\lambda} - \phi\right)\right]e^{-\frac{z}{\delta}} \tag{6.18}$$

with:

$$f_0 = \frac{16\pi}{\lambda}\frac{[n^2(n^2+k^2-1)^2 + k^2(n^2+k^2+1)^2]^{1/2}}{[(n+1)^2+k^2]^2} \tag{6.19}$$

and

$$tan\phi = \frac{k(n^2+k^2+1)}{n(n^2+k^2-1)} \tag{6.20}$$

The spatial shape of the sensitivity function is plotted in figure 6.4 using the values of the photoelastic constants as deduced from the fit of the first acoustic phonon echo in the

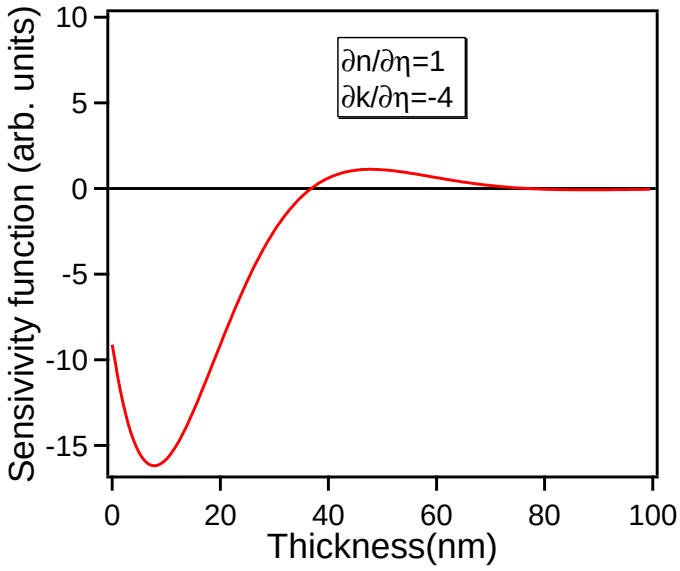

Figure 6.4: The shape of the sensitivity function for the Y(0001) case as determined using eq. 6.18 and the displayed values of the photoelastic constants.

figure 6.10. From here we see that the linear reflectivity will detect strain pulses that are localized in a range equal to maximum twice the optical penetration depth δ=28.68 nm.

Expression 6.17 is used for the simulation of the first phonon echo peak [178, 179] in the transient linear reflectivity measured from the Y(0001) films.

6.3 Acoustic phonons in yttrium

The phenomenon of travelling acoustic phonons has been studied for various Y(0001) film thicknesses employing the time-resolved linear reflectivity and second-harmonic generation. The measurements have been performed at a sample temperature of 90 K. The preparation of the thin Y(0001) films has been done in a similar manner as for Gd(0001) films namely deposition on the W(110) substrate held at room temperature and a subsequent annealing to 680 K for 10 minutes. The crystalline quality of the film has been checked with LEED.

A typical measurement showing the linear and nonlinear optical response from a 10 nm Y(0001) film with the laser tuned to 775 nm (for reasons that are apparent later) and at T=90 K is displayed in the figure 6.5. In the first place we notice the conspicuous peaks with alternating polarity in the linear reflectivity signal that are the signature of the travelling acoustic pulse. These are superimposed on a slowly decaying background that reflects (on this time scale) the cooling of the laser spot via thermal diffusion. The time evolution of the second-harmonic field resembles a comparable behavior as the linear reflectivity, with a sharp increase at early delays reflecting the increased temperature of the electronic bath and the subsequent relaxation to the lattice via *e-p* coupling (ps time

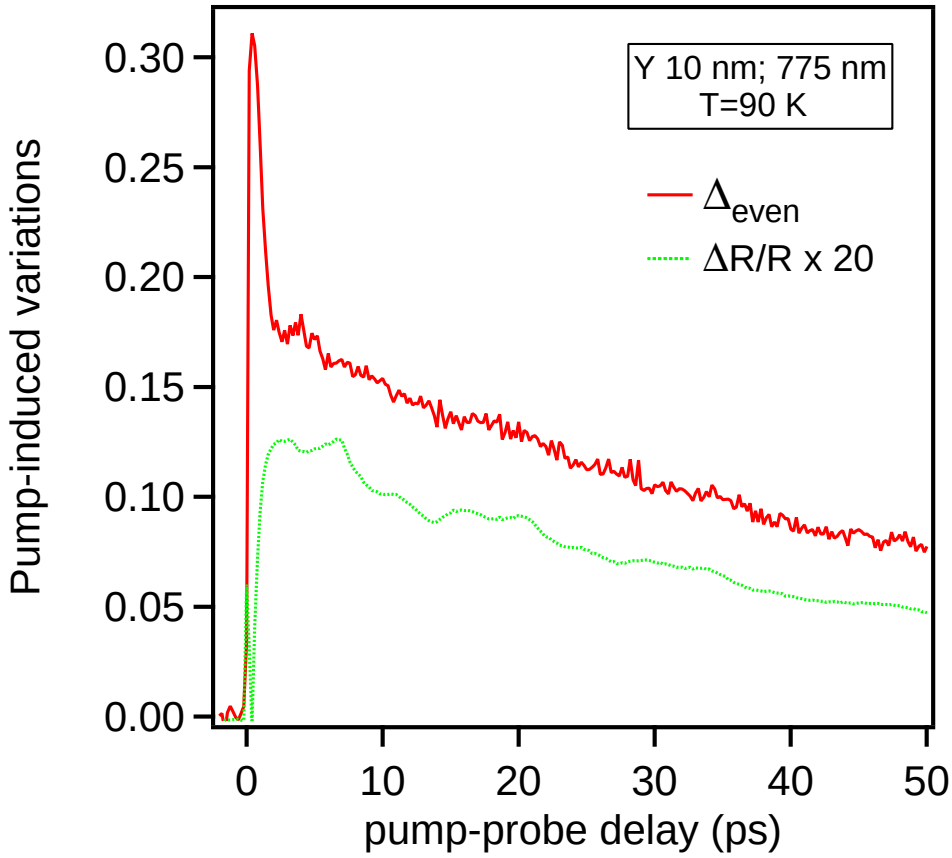

Figure 6.5: The time-resolved linear reflectivity (dotted line) and the second-harmonic (solid line) response from a 10 nm Y(0001) film, at a laser wavelength of 775 nm and T=90 K. Note the pronounced spikes in the linear reflectivity transient signal that reflect the phonon echo dynamics. The SHG signal lacks the phonon echo signature and shows a low signal to noise ratio due to the reduced efficiency of the SHG process on the Y(0001) surface (for details see text)

scale) as well as the cooling of the heated region via heat diffusion on a hundreds of ps time scale. Here we do not investigate in detail the behavior of the incoherent components of the time-resolved LR and SHG but we focus on the phonon echo dynamics. Regarding the excitation of coherent optical phonons on the Y(0001) surface, the transient SHG signal does not show the oscillatory signature of coherent lattice vibrations as was the case for Gd(0001). Also we could not resolve the phonon echoes in the SHG signal, although at the first glance one expects to observe such an effect due to the surface sensitivity of the SHG technique. We will come to these points later in this section.

As noticed from the raw data presented in figure 6.5, a lower signal to noise ratio is encountered in the transient SH field in comparison to the SHG response from Gd(0001) surface (see for example fig. 5.18). At the employed laser wavelength of 775 nm the probe beam SHG signal reaches ≈11 KHz (compared to typically 60–100 KHz from Gd(0001)),

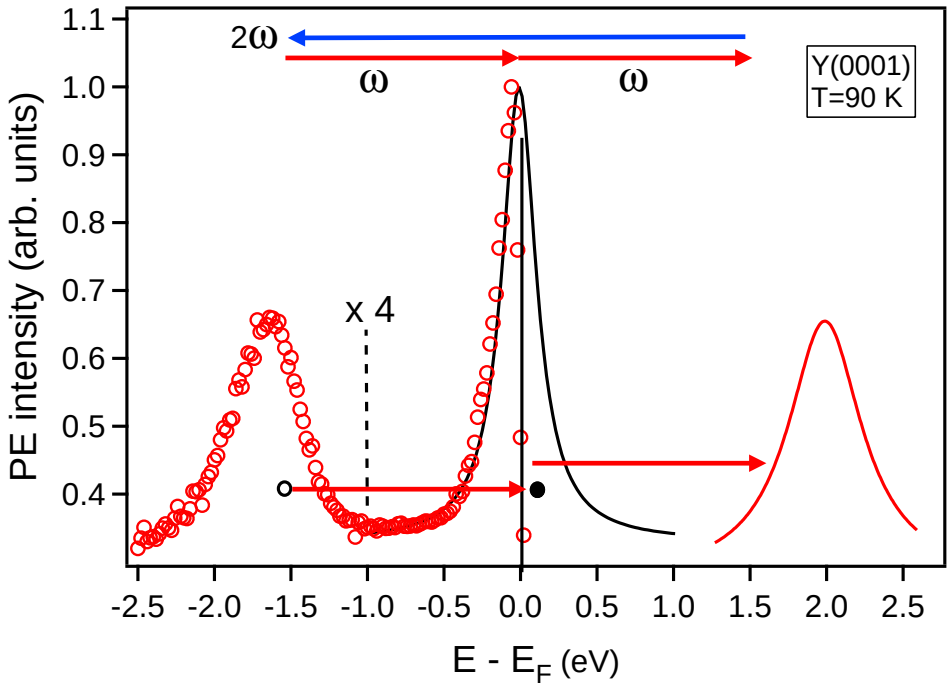

Figure 6.6: The valence electronic structure at $\overline{\Gamma}$ point for a 10 nm Y(0001) film at a temperature of 90 K. The arrows represent the pump-induced optical transitions (bottom) and the SHG probing mechanism (top). The occupied part of the electronic structure has been measured by O. Krupin (within the collaboration with our group) with photoemission at BESSY with synchrotron radiation of 36 eV beam energy at normal incidence. Note the position of the surface state that is positioned exactly at the E_F. The peak above Fermi level is a replica of the occupied bulk state centered at a energy of 2 eV, as reported in the literature [180].

that is the highest achievable SHG yield from the Y(0001) surface in the tunability range of the oscillator[1]: here 740 nm to 830 nm. The low SHG efficiency is determined by the the evolution of the SHG optical transitions via the electronic structure of Y(0001) presented in the figure 6.6.

Similar to gadolinium, Y(0001) exhibits a surface state that is now energetically located exactly at the Fermi level and is not exchange-split due to lack of ferromagnetic ordering of Y(0001) system. As shown in figure 6.6, the unoccupied (half) of the surface state acts as an intermediate level for the SHG optical transitions starting from the occupied bulk state centered at ≈1.65 eV below E_F. At 90 K the measured FWHM of the surface state amounts to ≈280 meV. Since at finite temperatures the unoccupied half of the surface state is partially populated by thermally excited electrons near E_F, the optical transition probability at the fundamental wavelength via the surface state is low and consequently the efficiency of the SHG process is weak. Above Fermi level, inverse photoemission

[1]These measurements have been performed before mounting in the laser oscillator mirrors with a broader bandwidth (see chapter 4).

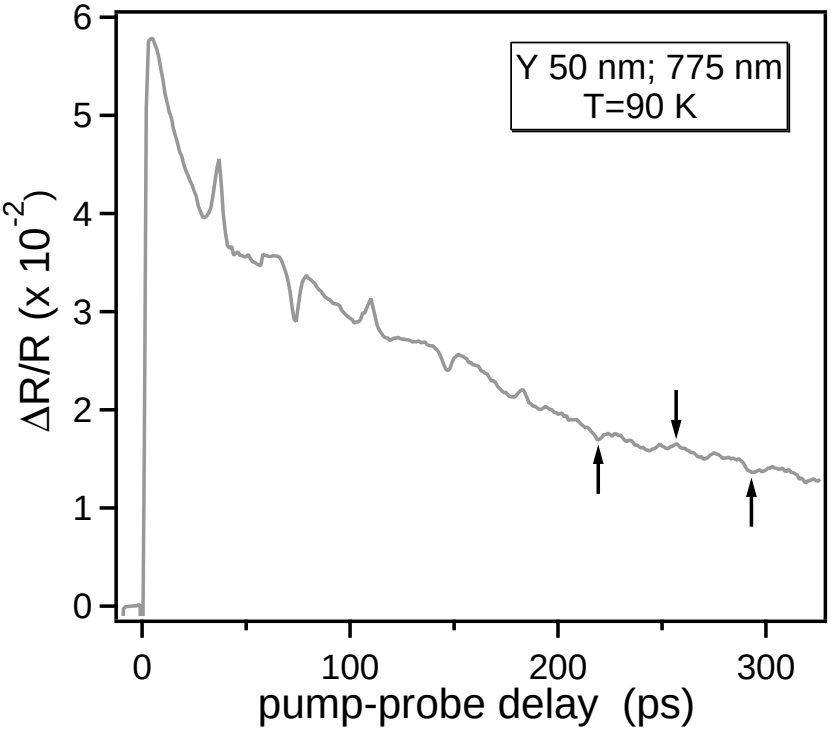

Figure 6.7: The time-resolved linear reflectivity measured on a 50 nm Y(0001) film at a laser wavelength of 775 nm and at a temperature of 90 K. Note the conspicuous peaks in the transient LR that reflect the propagating strain pulse within the film, that can be resolved up to the eighth echo. For clarity, the arrows are pointing the positions of the weaker intensity echoes.

measurements [180] performed at room temperature, show the existence of two features at 0.5± 0.2 eV and 2± 0.2 eV which have been ascribed to a surface state and unoccupied bulk state, respectively. The latter feature supports band structure calculations [181] of yttrium that at Γ point that give a value of 1.8 eV for the energetic position of the bulk state. From these results it is clear that the employed phonon energy in our experiment, between 1.5 eV to 1.65 eV, does not match the energetic separation between the measured surface state and the unoccupied bulk state, and thus the second optical transition involved in the SHG process evolves via a virtual state. Therefore the low SHG signal arising from the Y(0001) surface is explained by the low transition probability between the occupied bulk state and the half unoccupied surface state at the fundamental photon energy and the photon energy mismatch between the surface state and the unoccupied bulk state.

In the figure 6.7 the transient linear reflectivity measured from a 50 nm Y(0001) film is displayed. Here we can see clearly the dynamics of the propagating acoustic pulse with an alternating polarity, with the phonon echo signature resolved up to the eighth echo. The measured phonon echo is relatively long lived this fact being attributed to the special characteristics of the Y(0001)/W(110) system. First of all the acoustic reflection coefficient at the film/substrate interface r_{fs} amounts to 0.76 as deduced from eq. 6.10 using the

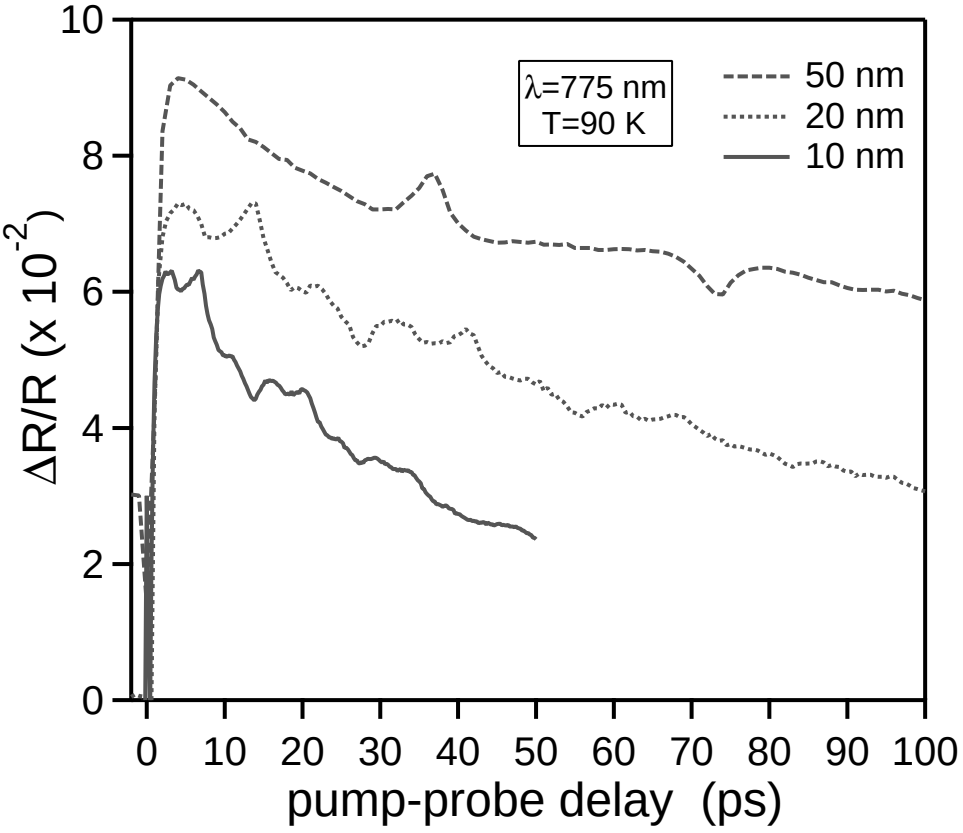

Figure 6.8: The dynamics of the phonon echo for various Y(0001) film thicknesses measured at 90 K. For clarity the transient LR for the 50 nm film is plotted with a positive offset along y axis.

acoustic impedances of bulk Y and W (see table 6.1). Secondly the optical absorption of the incident laser light is relatively high (R≈0.19 at λ=775 nm), that increases significantly the temperature of the irradiated region (see fig. 6.2) and consequently a high value of the initial strain that is launched into the film. Moreover, it seems that the film/substrate interface is smooth on the wavelength scale of the acoustic pulse, which prevents the distortion or deterioration of the propagating acoustic pulse. The good quality of the interface can be inferred from the UHV preparation conditions of the Y(0001) thin film.

Similar phonon echo transients are obtained for lower film thicknesses as can be seen in the figure 6.8. Here the measured LR dependencies for 10 nm and 20 nm film thickness are plotted together with the data for the 50 nm film, but on a shorter time scale (for clarity). A first information that can be deduced from the measured data of the figure 6.8 is either the thickness of the film or the sound velocity by measuring the time intervals between the echoes. A round trip that takes 36,5 ps within the 50 nm yttrium film while for the 20 nm and 10 nm it takes like 14 ps and 7 ps, respectively. From these data one obtains a sound velocity s=2816±55 m/s or accounting for the bulk sound velocity [182] s_{th}=3300 m/s one deduces a film thickness of 59.4 nm, 23.1 nm and 11.5 nm. Accounting

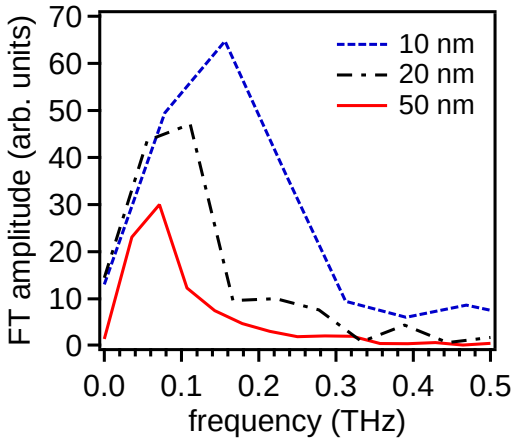

Figure 6.9: The frequency content obtained by Fourier transforming the first echoes measured on various Y(0001) film thicknesses. Note the higher frequencies 156 GHz and 111 GHz of the pulses obtained for lower thicknesses 10 nm and 20 nm, respectively, that are smaller than the penetration depth.

for the 10% error in thickness reading and the lack of reliable thin film single-crystals data we can say that is a relatively good agrement between the measured and predicted value for the sound velocity.

Another important piece of information that can be retrieved from the data is the value of the optical penetration depth δ. Taking into account the scattering of the optical constants data reported in literature, this is an useful insight from the experiment. The penetration depth can be deduced from the temporal extent of the acoustic pulses for different thicknesses. As long as the investigated thicknesses are smaller than δ, the shape and the temporal extent of the phonon echo is determined just by the film thickness (see eq. 6.4). Thus, smaller the thickness narrower is the pulse width in time and broader is the frequency content of the propagating strain pulse. The latter feature can be seen in the figure 6.9 where the Fourier transform of the first phonon echoes measured on different film thicknesses is displayed. For the 10 nm and 20 nm film thicknesses, that are lower than the penetration depth, higher frequency pulses are launched with central frequencies around 156 GHz and 111 GHz, respectively.
The skin depth can be deduced since together with the sound velocity of the material are the only quantities (in a first approximation) that limit the rise time of the lattice thermal expansion and implicitly the strain pulse duration. Accounting for the literature data [183] of the refractive index for bulk Y at 775 nm the calculated value of δ is 28.7 nm. Assuming this value to be close to the real one we should see no change in the duration of the acoustic pulse starting to this film thickness. Unfortunately no measured data is available for thicknesses between 20 nm and 50 nm, and thus we take the acoustic pulse duration value of the 50 nm measurement that amounts to 14 ps (for 10 nm and 20 nm the pulse duration is 6.4 ps and 9 ps respectively). This value together with the measured sound velocity of $\approx$2816 m/s results in a optical penetration depth $\delta \approx$39 nm. One can

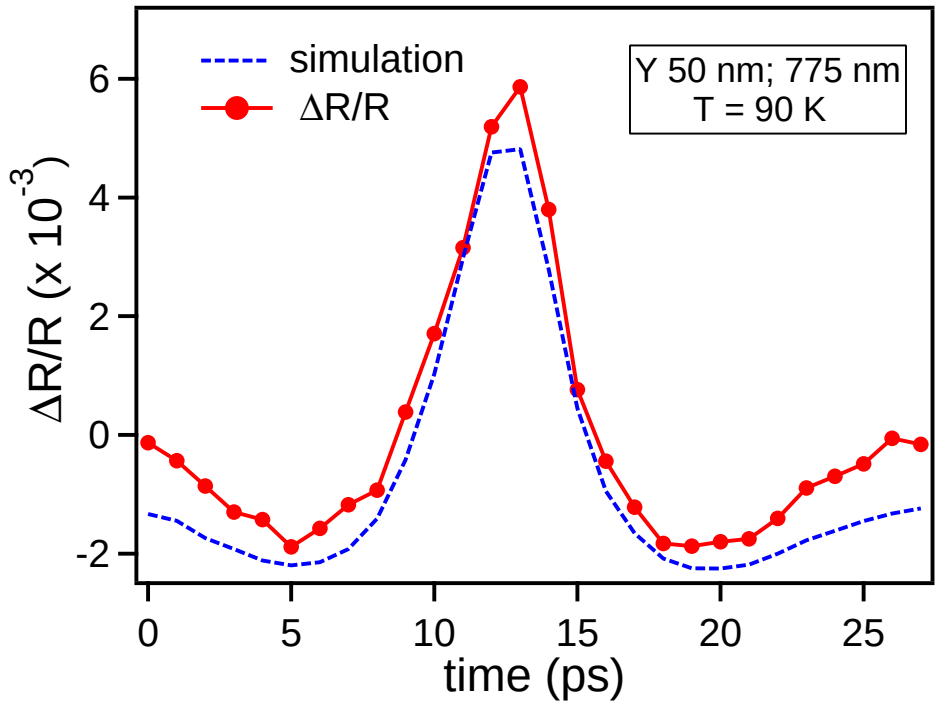

Figure 6.10: The first phonon echo measured on a 20 nm Y(0001) film together with the fit according to the thermoelastic model presented in section 6.2. The simulated phonon echo cannot account for the additional broadening of the measured phonon echo, since the thermoelastic model neglects the thermal diffusion that can make the strain pulse broader [178].

take this value as the optical penetration depth if, within the rise time of the strain pulse, the spatial extent of the energy transport (ballistic, electron diffusion, heat diffusion) is smaller than the obtained value of δ. Otherwise one obtains the depth that contributes to the generation of the strain pulse. For yttrium using the strain rise time τ of 14 ps and the defined diffusion length $l_{diff} = \sqrt{D\tau}$ from section 6.2 one obtains l_{diff}=13.3 nm, which is smaller than δ.

From the thickness-dependent data we can evaluate the value of the acoustic reflection coefficient from the magnitude ratio of subsequent phonon echo peaks. For an accurate determination of the reflection coefficient, the incoherent background has been removed from the raw data and the remaining part, reflecting the propagating strain pulse, is squared. From the ratios of subsequent peaks magnitude we get a value of r_{fs}=0.69±0.061 for the acoustic reflection coefficient of the Y(0001)/W(110) system, that agrees with the calculated one of 0.76. We have to keep in mind that the decrease of the phonon echo magnitude is partially determined also by the acoustic attenuation of the strain pulse in the film, which is not included in the definition of r_{fs}. By comparing the calculated and measured values of r_{fs} one can infer a good crystalline quality of the film with less defects.

In the figure 6.10 the first phonon echo measured on a 50 nm Y(0001) film is plotted together with the simulated one based on the thermoelastic model presented in section

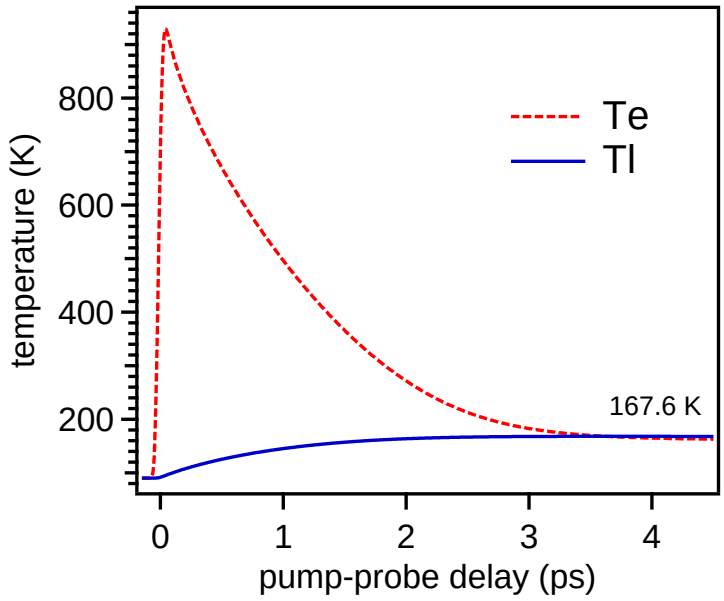

Figure 6.11: The evolution of the electronic T_e (dashed line) and lattice T_l (solid line) temperatures for a Y(0001) thin film as calculated with the two-temperature model [45] (see chapter2). Using an initial static temperature of 90 K, the increase of the system temperature after *e-p* equilibration reaches 167.6 K.

6.2. We notice a general good agreement between the measured and the simulated phonon echo but the latter one cannot account for the entire measured pulse width. This is due to the fact that the thermoelastic model assumes a instantaneous temperature increase upon laser pulse absorption neglecting any energy transport (ballistic, electronic diffusion or heat diffusion) out of the irradiated region as well as the heat diffusion. As a result the spatial extent over which the energy is distributed can be larger than the optical penetration depth and consequently the phonon echo pulse width is broader than initially estimated by the thermoelastic model. This might be also our case since the estimated temperature increase according to thermoelastic model is 160 K while calculated with the two-temperature model, that accounts for electronic diffusion, is just ≈80 K at the electron-phonon equilibration time. The computed[2] electronic and lattice temperatures according to 2TM are plotted in the figure 6.11. However, for an accurate theoretical description of the photo-generated strain pulse in metals and semiconductors the energy transport effects out of the irradiated region during the rise time of the strain pulse should be included in the framework of the thermoelastic model.

Finally we address the lack of the coherent optical phonons and of the phonon echoes in the transient SHG signal. As showed earlier in this section the efficiency of the pump-induced optical transitions over the partially empty surface state of Y(0001) is small. As a result the excited electron population at the surface cannot trigger coherent lattice

[2]The used parameters in the computation using 2TM are Θ_D=256 K, electron heat capacity γ=300 J/m^3K^2 [53] and the electron-phonon coupling constant g=1·10$^{17}W/m^3K$ [58].

vibrations. Regarding the lack of the phonon echo dynamics in the SHG response, this can be ascribed to the symmetry of the strain tensor. The strain is described by a second rank tensor [98] and therefore cannot be detected with second-harmonic generation or any nonlinear effect that is sensitive to properties described by odd rank tensors. In this context the third-harmonic generation would be sensitive to the propagating strain dynamics. Also the SHG probes a spatial region limited to the first atomic layers and thus not sensitive to the entire strain pulse. Another possibility would be that the photoelastic constants have small variations in the SH frequency range.

At this point a comparison between the phonon echo on Y(0001) and Gd(0001) systems would be intersecting. Calculating the acoustic reflection coefficient for Gd one obtains a value of 0.65 and thus big enough that a presumably excited strain pulse to be reflected at the interface and eventually detected. As can be seen in the figure 5.18 no signature of the phonon echo could be detected on Gd(0001). The crystalline quality of the Gd(0001) film is assumed to be at least comparable to that of Y(0001) (from LEED pictures) and the same holds also for the film/substrate interface (Gd and Y have almost identical lattice constants). One explanation is that the optical constants of Gd film are less sensitive to the presence of strain. Therefore the strain induced changes of the optical response (the sensitivity function) are very small and cannot be detected.

6.4 Influence of the laser wavelength and temperature

This section addresses the effect of the laser wavelength and the temperature variation of the sample on the phonon echo dynamics on Y(0001)/W(110). A wavelength-dependent study of the phonon echo is always required taking into account the dependence of the sensitivity function (see eq. 6.18) on the probing laser wavelength and the fact that the photoelastic constants might change with the wavelength. As for the temperature dependence, upon increasing the temperature the lattice expands and simultaneously the thermal phonons population is increased, both affecting the sound velocity of the material and implicitly the propagating strain pulse.

Wavelength dependence

Here we investigate the effect of the laser wavelength on the phonon echo dynamics measured from Y(0001)/W(110). For this purpose the wavelength of the laser is varied between 750 nm to 825 nm with the sample held at 90 K. As mentioned above, the laser wavelength determines the magnitude and the spatial profile of the sensitivity function through equation 6.18, that influence the detection of the strain pulse (see section 6.2). Simultaneously the photoelastic constants can vary with the laser photon energy and thus affecting the amplitude of the detected change in the linear reflectivity caused by the presence of travelling strain pulse (see eq. 6.13). Moreover the optical penetration depth changes with the wavelength, that results in different spatial extents of the generated strain pulse.

The wavelength dependence measured from a 20 nm Y(0001) film is shown in the figure 6.12. We notice that varying the laser wavelength no change in the shape of the phonon echoes is produced, contrary to what has been reported in literature [179, 184, 185] for various systems. We have to mention here that larger wavelength ranges have been employed

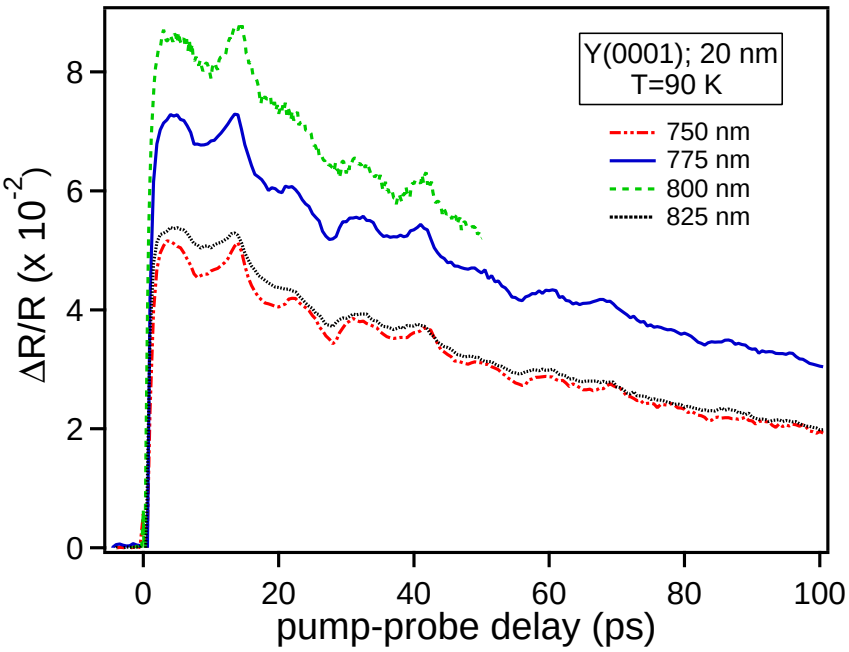

Figure 6.12: The pump-induced variations in the linear reflectivity for various laser wavelengths measured from a 20 nm Y(0001)/W(110) film at T=90 K. The transient LR measured at λ=800 nm is recorded with a higher density of data points on a shorter delay time scale.

in the above cited works. However, a wavelength-dependent variation in the magnitude of the phonon echo peaks is encountered. This can be clearly observed in the figure 6.13, where the LR signal arising from the propagating strain pulse is plotted after removing of the incoherent background. From here we see a variation of ≈50% in the phonon echo magnitude upon changing the laser wavelength. Also the change in magnitude of the phonon echoes with wavelength exhibits a non-monotonous behavior: the peak amplitude is higher for the central wavelengths (800 nm and 775 nm) and decreases for the limit wavelengths (750 nm and 825 nm).

As for the magnitude of the phonon echoes, a non-monotonous wavelength-dependent change appears in the absolute values of the pump-induced variations of the incoherent background. Inspecting the raw data in the figure 6.12, we notice a similar value for the incoherent background of the LR transients measured for 825 nm and 750 nm, while larger values are measured for 775 nm and 800 nm data sets. The incoherent part of the linear reflectivity reflects the initial photoexcited electron population that transfers energy to the lattice via *e-ph* coupling (sub-picosecond time scale) and the subsequent cooling of the lattice through heat diffusion. Thus for the 775 nm and 800 nm measurements the the absorbed energy density is higher than for the limit wavelengths 750 nm nd 825 nm. The source term that describes the absorbed energy density (eq. 6.2) becomes dependent only on the reflectivity value R when the penetration depth is smaller than the film thickness, which is our case. Calculating the reflectivity values based on literature values for the

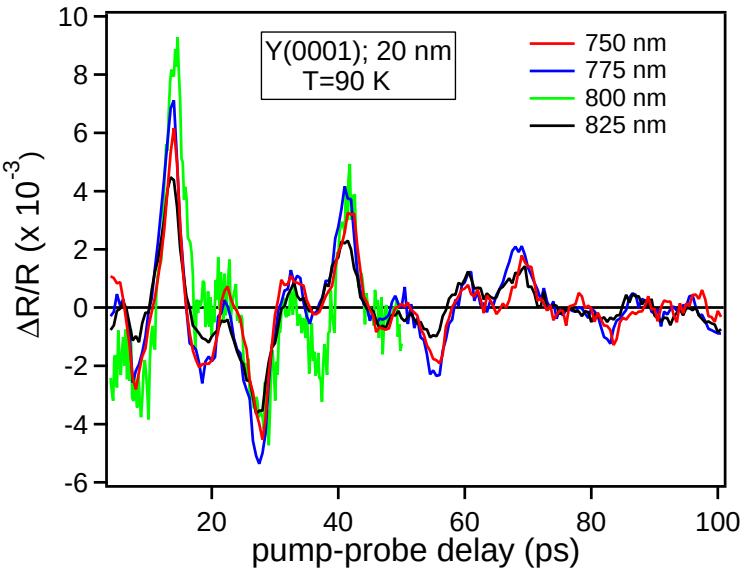

Figure 6.13: The wavelength dependence of the linear reflectivity part reflecting the propagating acoustic pulse obtained after substraction of the incoherent background. No change in the shape of the phonon echo shape is observed upon varying the wavelength.

refractive index [183], one obtains a monotonous decreasing of the reflectivity from ≈0.24 to ≈0.17 by increasing the wavelength from 750 nm to 825 nm, respectively. Hence the highest absorption value would be for a laser wavelength of 825 nm and thus the highest pump-induced variations of the incoherent LR are expected for this laser wavelength. Instead we observe a similar incoherent background level as for the 750 nm data set. This behavior suggests that an additional mechanism should be involved in the initial optical absorption and implicitly excitation of the system. It might be that the unoccupied part of the surface state present on Y(0001) (see fig. 6.6) is responsible for this non-monotonous behavior observed in the phonon echo and the incoherent LR dynamics. It seems that for the lowest and the highest laser wavelengths used here (750 nm and 825 nm) the photon energy does not match the unoccupied part of the surface state, whereas for the central wavelengths a better photon energy matching takes place. Hence an additional absorption process of the fundamental photon might take place via the surface state. As an experimental input that supports this allegation is the wavelength-dependent SHG (a process sensitive to surface electronic structure see the previous chapter) signal displayed in figure 6.14, that increases for these central wavelengths. However, in order to check this proposal further measurements are needed with a smaller step variation in the laser wavelength and covering a broader wavelength range.

Summarizing, within the investigated laser wavelength range between 750 nm and 825 nm we do not observe major changes in the phonon echo dynamics. Beside a variation in the magnitude of the detected echoes that depends on the laser photon energy being more pronounced for central wavelengths (775 nm and 800 nm), no change in their shape is noticed. The same trend with the change of the laser photon energy is encountered in

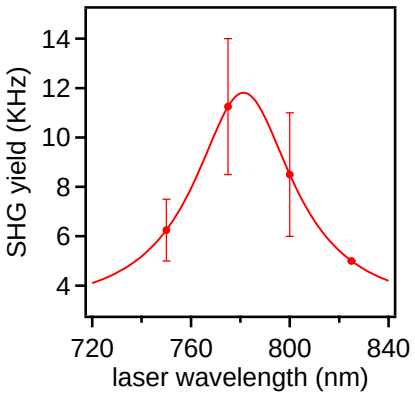

Figure 6.14: The variation of the SHG signal with the wavelength of the fundamental laser beam. The data points are fitted with a lorentzian centered around 780 nm.

the pump-induced variations of the incoherent background, that points to a more efficient optical excitation for the 775 nm and 800 nm wavelengths. Since the encountered behavior is non-monotonous *i.e.* for the highest and lowest photon energies the transient LR are similar (see fig. 6.12), this suggests that the surface state might play a role in the optical excitation of the system and the generation of the strain pulse.

Temperature effects

The effect of the temperature variation on the phonon echo dynamics measured on 10 nm Y(0001) film is presented in the figure 6.15. Here the measured time-evolution of the linear reflectivity is shown for three representative temperatures. We notice that the LR transients exhibit a qualitatively similar behavior upon temperature increase, with the absolute level of pump-induced variations of the incoherent background decreasing with increasing temperature. Simultaneously the magnitude of the phonon echoes peak is slightly decreasing by elevating the temperature. The latter behavior is better seen in the figure 6.16, where the contribution to the LR arising from the propagating acoustic pulse, obtained after background subtraction, is plotted for the employed temperatures. Within the investigated temperature range the decrease of the phonon echo peak is linear with the temperature increase. This can be seen from the figure 6.17, where the magnitude of the phonon echoes is displayed versus temperature for the first three echoes of the strain pulse (due to their better statistics).

Another feature that can be observed upon temperature increase is the fact that the phonon echoes arrive at the surface temporally delayed with respect to the detected echoes measured at low temperature. This can be clearly seen for all five echoes in figure 6.16. By evaluating the difference in the arrival time of the strain pulse for different temperatures one can calculate the variation of the sound velocity as a function of temperature. We measure a positive delay in the arrival time of the phonon echoes around 0.2 ps for each step in the temperature increase, that results in a decrease of the sound velocity of $\approx$6% at 400 K in comparison with the low temperature data. In order to have a complete picture about the temperature-dependent sound velocity and acoustic attenuation, the investigated temperature interval should be extended up to temperatures at which the phonon echoes can not be detected anymore. Also a higher density of data points in the

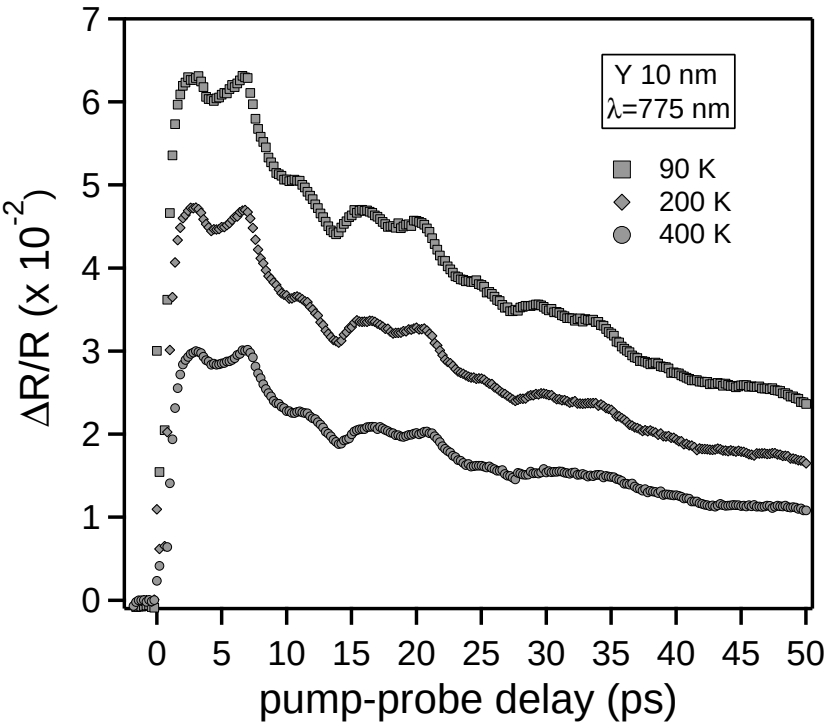

Figure 6.15: The temperature dependence of the phonon echo dynamics measured on a 20 nm Y(0001) film at a laser wavelength of 775 nm.

temperature dependence are needed. Therefore more detailed measurements would be useful in this context.

The temperature-dependent variation of the sound velocity is determined by two factors: the thermal expansion of the material and the increased thermal phonon population. The effect of the first factor is straightforward since an increased thermal expansion produces an additional strain of the lattice and thus affecting the sound velocity of the specimen. Regarding the second factor the increased phonon population affects the travelling sound wave by anharmonic interactions where a longitudinal acoustic phonon *i.e.* the propagating strain pulse scatters into two transversal (thermal) phonons with the conservation of energy and momentum. In principle more phonons can be involved in the decay of the longitudinal acoustic phonon but these are higher order effects and usually appearing with a lower probability. One way to disentangle between the anharmonic decay and the thermal expansion contribution to the temperature-dependent decrease of the sound velocity relies on the fact that the first contribution depends on the frequency of the acoustic pulse while the other not. Moreover the thermal expansion gives a linear dependence of the sound velocity on the temperature. Unfortunately, due to the lack of higher density of data points we could not perform a detailed analysis in order to identify the source of the sound velocity variation with temperature.

Summarizing, upon increasing the temperature the phonon echo magnitude decreases

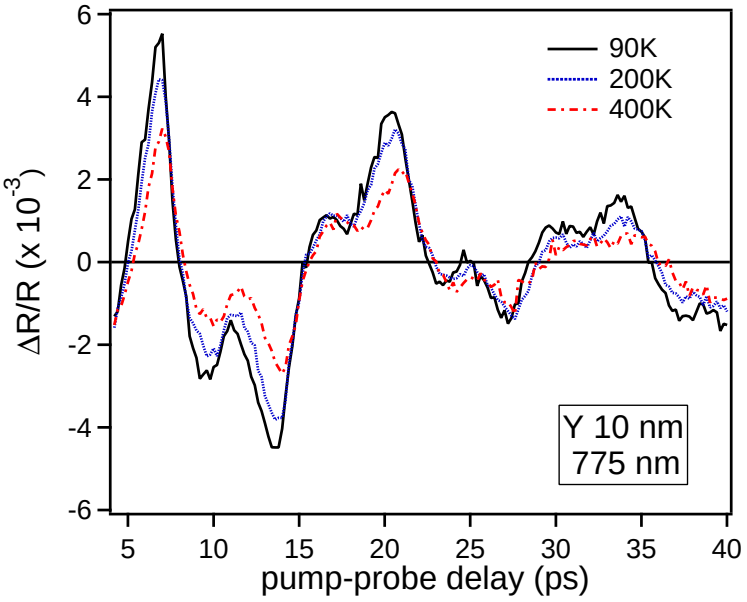

Figure 6.16: The variation of the linear reflectivity signal arising from the propagating strain pulse with the temperature. Note that increasing the temperature the phonon echo peaks shift to longer delay times.

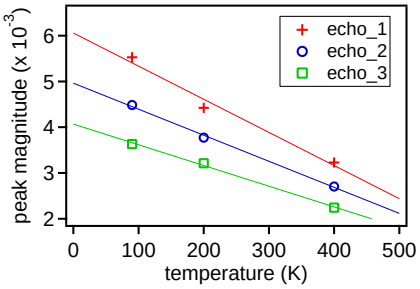

Figure 6.17: The temperature-dependent variation of the magnitude of the phonon echo peaks measured for the first three echoes. The solid lines are linear fits to the data.

linearly and simultaneously the sound velocity decreases by ≈6% in comparison to the low temperature value. The processes responsible for the temperature-dependent sound velocity behavior have been discussed but due to the lack of higher density of measured data points their contribution could not be separated.

6.5 Conclusions and outlook

In this chapter preliminary results regarding the laser-induced dynamics on the Y(0001) thin films have been presented, employing as investigation tools time-resolved linear reflectivity and second-harmonic generation. Upon laser excitation the time-resolved linear reflectivity shows pronounced "spikes" with alternating polarity which appear at constant time intervals in the transient signal, that have been interpreted as propagating acoustic phonons in the Y(0001) film. These phonon echoes are relatively long lived due to the high

optical absorption of the material, the high value of the acoustic reflection coefficient of the Y/W interface and presumably due to the smoothness of the buried interface region. The frequency content of the acoustic pulses is ranging from 70 GHz to 156 GHz (central frequency), that can be varied by employing different film thicknesses smaller than the optical penetration depth. From the phonon echo dynamics measured on various Y(0001) film thicknesses we could accurately measure the sound velocity, the optical penetration depth and the actual film thickness. Moreover we could determine the photoelastic constants for yttrium by fitting the first phonon echo peak using the phenomenological thermoelastic model. In this context an extension of the thermoelastic model using a transfer matrix method for the simulation of the entire travelling path of the strain pulse would be useful. Although a good reproducibility of the first phonon echo with the actual model could be obtained, the integration of the electronic energy transport into the model would account for the additional broadening of the pulse determined by the heat diffusion. Upon varying the laser wavelength the magnitude of the phonon echoes changes with no modification in the shape of the travelling strain pulse, which means that the photoelastic constants do not change significantly within the employed wavelength range. Increasing the temperature of the sample the sound velocity of the propagating acoustic pulse changes due to the combined effect of the thermal expansion and increased thermal phonon population. We could not resolved the phonon echo signature in the second-harmonic signal arising from the Y(0001) surface presumably due to small changes of the photoelastic constants in the SH frequency range, the restricted probing depth to the surface region and the symmetry of the strain. This is described by a second rank tensor and thus can not be detected with second-harmonic or any nonlinear tool sensitive to odd rank tensors. In this context the third-harmonic generation would be able to detect the changes in the optical susceptibility of the sample by the propagating strain pulse. Also the excitation of the coherent optical phonons on the Y(0001) surface could not done due to the specificity of the surface state positioned at E_F, that does not allow an efficient excitation of the system.